ORIGINAL PAPER

Aerodynamic roughness of the sea surface at high winds

Vladimir N. Kudryavtsev · Vladimir K. Makin

Abstract The role of the surface roughness in the formation of the aerodynamic friction of the water surface at high wind speeds is investigated. The study is based on a wind-over-waves coupling theory. In this theory waves provide the surface friction velocity through the form drag, while the energy input from the wind to waves depends on the friction velocity and the wind speed. The wind-over-waves coupling model is extended to high wind speeds taking into account the effect of sheltering of the short wind waves by the air-flow separation from breaking crests of longer waves. It is suggested that the momentum and energy flux from the wind to short waves locally vanishes if they are trapped into the separation bubble of breaking longer waves. At short fetches, typical for laboratory conditions, and strong winds the steep dominant wind waves break frequently and provide the major part of the total form drag through the air-flow separation from breaking crests, and the effect of short waves on the sea drag is suppressed. In this case the dependence of the drag coefficient on the wind speed is much weaker than would be expected from the standard parameterization of the roughness parameter through the Charnock relation. At long fetches, typical for the field, waves in the spectral peak break rarely and their contribution to the air-flow separation is weak. In this case the surface form drag is determined predominantly by the air-flow separation from breaking of the equilibrium range waves. As found at high wind speeds up to $60\,\mathrm{m\,s^{-1}}$ the modelled aerodynamic roughness is consistent with the Charnock relation, i.e. there is no saturation of the sea drag. Unlike the aerodynamic roughness, the geometrical surface roughness (height of short waves) could be saturated or even suppressed when the wind speed exceeds $30\,\mathrm{m\,s^{-1}}$.

Keywords Breaking wind waves · High wind conditions · Sea drag · Separation of the air flow

V. N. Kudryavtsev
Nansen International Environmental and Remote Sensing Center (NIERSC), Saint-Peterburg, Russia
Nansen Environmental and Remote Sensing Center (NERSC), Bergen, Norway

V. K. Makin (✉)
Royal Netherlands Meteorological Institute (KNMI), 3730AE, De Bilt, The Netherlands
e-mail: makin@knmi.nl

1 Introduction

A strong local enhancement of the surface stress above breaking waves was reported in a number of laboratory experiments (e.g., Banner and Melville 1976; Kawamura and Toba 1988; Banner 1990; Melville 1996; Giovanangeli et al. 1999; Reul et al. 1999). It has been argued that the air-flow separation (AFS) from the crest of breaking waves is responsible for this enhancement, which may in turn significantly contribute to the total form drag of the wavy surface. Kudryavtsev and Makin (2001) (hereinafter KM01), and Makin and Kudryavtsev (2002) (hereinafter MK02) proposed a model, which takes into account the impact of the AFS on the sea surface drag. They showed that the contribution of the AFS to the form drag rapidly increases with the wind speed, and at wind speeds 20–25 m s^{-1} the AFS supports about half of the total surface wind stress.

Wave breaking manifests itself in the form of white caps—an observable phenomenon on the sea surface. At high wind speeds and young seas white caps are formed very intensively that suggests that the AFS may play a dominant role in supporting the form drag of the sea surface. Donelan et al. (2004) investigated the aerodynamic roughness of the water surface at extreme wind speeds in laboratory conditions. They observed a saturation of the surface drag coefficient at the wind speed exceeding 33 m s^{-1}. As a plausible mechanism the separation of the air flow from continually breaking wave crests was suggested to explain this fact. A similar mechanism as the limiting regime of the form drag was also suggested by KM01. The experimental finding by Donelan et al. (2004) is similar to that found by Powell et al. (2003) in the open sea under hurricane wind speeds. Though both datasets indicate the saturation of the drag coefficient at the wind speed above 30–35 m s^{-1}, the physics lying behind this phenomenon could be quite different. In laboratory conditions this phenomenon, as was suggested by Donelan et al. (2004), could be explained by the saturation of the aerodynamic roughness due to the air-flow separation. While in the open field, where waves are not so short and steep as in laboratory conditions, a plausible mechanism is the impact of the sea droplets and the foam on the air-flow dynamics. Recent theoretical studies by Makin (2005), Bye and Jenkins (2006), and Kudryavtsev (2006) offer the physical grounds for the efficiency of this mechanism.

An adequate description of the exchange processes at the sea surface at high wind speeds is very important for the storm surge and the hurricane prediction. For example, the sensitivity study of the tropical cyclone model performed by Emanuel (1995) showed that cyclones cannot attain their observed intensity with the traditional parameterizations of the surface exchange coefficients, and to obtain that it is necessary to reduce the ratio of the drag coefficient to the enthalpy transfer coefficient. Makin (2005) and Kudryavtsev (2006) explored the impact of the sea droplets on the surface drag through the effect of the buoyancy force on the turbulent mixing. They showed that the efficiency of such a mechanism is sufficient to suppress the drag coefficient. However, both of these model approaches were based on the Charnock's parameterization of the aerodynamic roughness of the sea surface. Deviation of the aerodynamic roughness at high wind speeds from the Charnock relation may significantly affect the result.

The main goal of the present paper is focused on the aerodynamic roughness of the sea surface at high wind conditions. In this context, the present study complements the study by Makin (2005) and Kudryavtsev (2006), where the validity of the Charnock relation for the description of the aerodynamic roughness of the sea surface at high wind conditions was postulated. On the other hand, this study is essentially based on the KM01 and MK02 model, which is extended here to the case of high wind conditions when the intensive breaking of waves becomes a dominant surface feature. One may anticipate that at such conditions the

AFS from breaking wave crests on one hand will dominate the form drag, and on the other hand will reduce the form drag due to sheltering of some fraction of the sea surface. The latter results from the fact that the shorter waves could be sheltered by longer waves: being trapped in the separation bubble induced by the longer wave they do not extract momentum from the air flow and thus locally do not contribute to the form drag. In the present paper we present a model description of this effect and analyze its significance for high wind conditions when the wind seas are essentially undeveloped.

2 Form drag at intensive wave breaking

In KM01 the form drag τ_f of the sea surface was presented as a sum of the wave-induced stress τ_w (correlation of the surface pressure with the slope of the regular streamlined wavy surface) and the AFS stress τ_s, describing the action of the pressure drop on the surface slope discontinuity that models the wave breaking front: $\tau_f = \tau_w + \tau_s$. The spectral density of the form drag supported by the surface waves with the wavenumber from $\mathbf{k}$ to $\mathbf{k} + d\mathbf{k}$ reads:

$$d\tau_f(\mathbf{k}) = d\tau_w^0(\mathbf{k}) + d\tau_s^0(\mathbf{k}), \tag{1}$$

where the components of the form drag are

$$d\tau_w^0(\mathbf{k}) = c_\beta u_*^2 \cos^3 \theta k^{-2} B(\mathbf{k}) d\mathbf{k}, \tag{2}$$

$$d\tau_s^0(\mathbf{k}) = c_s u_*^2 \cos^3 \theta k^{-1} \Lambda(\mathbf{k}) d\mathbf{k}. \tag{3}$$

In these equations c, k and θ are the phase velocity, the wavenumber and its direction; u_* is the friction velocity; c_β is the growth rate coefficient defined as $c_\beta = 1.5\kappa^{-1} \ln(\pi/(kz_c))$; $B(\mathbf{k})$ is the saturation spectrum; $\Lambda(\mathbf{k})d\mathbf{k}$ is the length of wave breaking fronts per unit area; $c_s = \varepsilon_b \gamma / \kappa^2 \ln^2(\varepsilon_b/(kz_c))$ is the separation stress coefficient; $\kappa = 0.4$ is the von Karman constant; $\varepsilon_b = 0.5$ is the characteristic steepness of the breaking wave; $\gamma \sim 1$ taken here as 0.75 is an empirical constant relating the pressure drop in the separation bubble to the airflow velocity; $z_c = z_0 \exp(\kappa c/(u_* \cos \theta_b))$ is traditionally referred to as the height of the critical layer, and z_0 is the surface roughness parameter. Integration of (1) over all $\mathbf{k}$ at specified $B(\mathbf{k})$ and $\Lambda(\mathbf{k})$ gives the total surface form drag τ_f. The solution of the momentum conservation equation

$$u_*^2 = \tau_f + \tau_v, \tag{4}$$

where τ_v is the viscous surface stress

$$\tau_v = \frac{1}{\kappa d} \ln\left(\frac{d\nu}{z_0 u_*}\right) u_*^2, \tag{5}$$

(ν is the molecular viscosity and $d = 10$ is the molecular sub-layer constant) provides the drag coefficient of the sea surface. It was shown that the model results are consistent with the observations at low and moderate wind speeds.

KM01 and MK02 restricted their analysis to low and moderate wind conditions, when the fraction of the sea surface covered (or sheltered) by the separation bubbles is relatively small. However, at high wind speeds this assumption may lose its validity. Let us assume that the surface waves are quasi-monochromatic with the wavenumber k_p and the probability of the wave crest breaking P_p. Then the total length of breaking crests per unit surface is

$$L_p \equiv \Lambda(\mathbf{k})d\mathbf{k} = \frac{k_p}{2\pi} P_p. \tag{6}$$

The air flow separates from the breaking crest and reattaches to the surface on the up-wind slope of the downwind wave, closer to its crest. Thus the individual breaking crest with the length l_i shelters the area q^i proportional to $q^i \sim 2\pi/k_p l_i$, and the total fraction of the sea surface sheltered by all breaking crests $q_p = \sum q^i$ is

$$q_p = 2\pi/k_p L_p = P_p. \tag{7}$$

The action of the pressure drop inside the separation bubble on the breaking front was already included in the definition of the separation stress. Therefore the sheltered surface area should be excluded from the wave-induced momentum flux, and the expression for the form drag now reads:

$$\tau_f^p = \tau_s^p + (1 - q_p)\tau_w^p.$$

KM01 and MK02 assumed that $q_p \ll 1$ and therefore the form drag is simply the sum of τ_w and τ_s, Eq. 1. The assumption is reasonable for low and moderate wind conditions when wave breaking occurs relatively rare, but it certainly breaks down at high and extreme wind speeds when the intensive wave breaking becomes a dominant surface feature.

Let us consider the extreme case when slow waves with $c_p \ll u_{10}$, where u_{10} is the wind speed at the reference level of 10 m height, are so steep that each of their crest breaks: $P_p = 1$ and $q_p = 1$. In this case the surface stress is fully supported by the AFS: $u_*^2 = \tau_s^p$. Then, taking into account the expression (3) for the AFS stress, and L_p defined by (6) at $P_p = 1$, we have the following equation for the sea-surface roughness parameter z_0:

$$z_0/h_p = \frac{1}{2} \exp\left(-\kappa\sqrt{\frac{2\pi}{\varepsilon_b \gamma}}\right), \tag{8}$$

where $h_p = 2\varepsilon_b/k_p$ is the height of the breaking wave. At $\varepsilon_b = 0.5$ in the range of γ from 0.25 to 1 the roughness parameter varies from $z_0/h_p = 0.03$ to $z_0/h_p = 0.1$, i.e. approximately from 1/30 to 1/10 of the height of the roughness element. This estimate is consistent with the classical empirical knowledge (Monin and Yaglom 1971).

For the real wind seas the surface waves are not narrow, and we introduce the cumulative fraction of the sheltered surface

$$q(k) = 2\pi \int_{k_1 < k} \cos\theta k_1^{-1} \Lambda(\mathbf{k}_1) d\mathbf{k}_1 \tag{9}$$

describing the cumulative contribution of breaking wind waves to the sheltered zones. We suggest that there is a cascade sheltering, i.e. the AFS from the breaking crest of longer waves shelters the shorter waves and thus prevents the wave-induced momentum flux to these shorter waves that are trapped in the sheltered zone. In terms of the cumulative fraction of the sheltered surface, the wave-induced component of the form drag can be written as:

$$d\tau_w(\mathbf{k}) = (1 - q(k))d\tau_w^0(\mathbf{k}), \tag{10}$$

where $d\tau_w^0(\mathbf{k})$ is the wave-induced momentum flux described by (2).

One may anticipate that at high wind speeds, when the wave breaking of waves of different scales is strongly intensified, the AFS from the long breaking waves may shelter the shorter breaking waves. In other words, there is an overlapping of the sheltered area generated by the AFS from the breaking crest of different wave scales. This may lead to the fact that the fraction of the sheltered zones will be more than unity $q(k) > 1$ at some wavenumber exceeding a threshold value $k > k_o$, where k_o is the overlapping wavenumber defined as the solution of the equation $q(k_o) = 1$. Precise description of the statistics of the overlapping

sheltered areas is out of the scope of the present study. Instead, in order to take into account this effect on a qualitative level, we simply assumed that the AFS from the breaking crest of waves with the wavenumber $k > k_o$ do not contribute to the total AFS stress τ_s since their separation bubbles are absorbed by the separation bubbles induced by longer waves. Thus the AFS stress can be written as

$$d\tau_s(\mathbf{k}) = h(k_o - k)d\tau_s^0(\mathbf{k}), \tag{11}$$

where $d\tau_s^0(\mathbf{k})$ is the AFS stress described by (3), and $h(x)$ is the Heaviside step-function: $h(x) = 0$ at $x < 0$ and $h(x) = 1$ at $x > 0$.

3 Surface drag

The experiment by Reul et al. (1999) revealed the intensive vortex inside the separation bubble that produces near the surface a counter flow with the velocity of about 20% of the wind velocity in the free stream. This presumes that contrary to the "regular surface", the viscous surface stress inside the sheltered area could be negative. However, taking into account that the stress is proportional to the square of the wind speed, we shall ignore this negative contribution, which is small (of order $0.04q$) relative to the non-separated fraction of the surface. Therefore, the total surface stress in the case of intensive wave breaking at high wind speeds reads

$$\int (1 - q(k))d\tau_w^0(\mathbf{k}) + \int_{k<k_b} h(k_o - k)d\tau_s^0(\mathbf{k}) + (1 - q(k_b))\tau_v = u_*^2, \tag{12}$$

where $k_b \simeq 2\pi/0.15$ rad m^{-1} is the wavenumber of the shortest breaking wave, which provides the AFS. As discussed by KM01, the generation of parasitic capillaries by shorter breaking waves prevents the air-flow separation. Notice, that q in (12) is limited by the value 1, i.e. $q(k) = \min(q(k), 1)$. If $q(k_b) \ll 1$ the model described by KM01 is retrieved.

To complete the problem one needs to define $\Lambda(\mathbf{k})$ describing the length of the wave breaking front. In the equilibrium range of the spectrum, KM01 defined this quantity following the approach proposed by Phillips (1985). The quantity $\Lambda(\mathbf{k})$ defines the spectral energy loss $D(\mathbf{k})$ due to wave breaking

$$D(\mathbf{k}) = bg^{-1}c^5\Lambda(\mathbf{k}), \tag{13}$$

where b is an empirical constant of order $b \sim 10^{-1} - 10^{-2}$ (see, for example, references in KM01, and the discussion by Babanin and Young (2005) for more details; we mention here that the exact value of b is not important for the present study as b appears in the expression for the separation stress, Eq. 20 below in the text, in combination with other constants, and only their combined value is relevant for the model results). Since in the equilibrium range D is proportional to the wind energy input $I(\mathbf{k})$

$$D(\mathbf{k}) \sim I(\mathbf{k}) = \beta\omega g k^{-4}B(\mathbf{k}) \tag{14}$$

then, combining (13) and (14), the following equation for $\Lambda(\mathbf{k})$ is obtained

$$\Lambda(\mathbf{k}) \sim b^{-1}\beta k^{-1}B(\mathbf{k}). \tag{15}$$

In developed seas, the main contribution to the total length of wave breaking fronts comes from the shortest breaking waves (Phillips 1985), and the role of dominant waves (waves in the spectral peak) in supporting the form drag is negligible (see KM01 for more details).

The present study is focused on high wind conditions, when wind seas are most likely undeveloped. MK02 gave an estimate of the impact of the AFS from the dominant waves on the sea drag for young seas. Adopting the threshold level approach proposed by Longuet-Higgins (1957), they found quite a strong effect of the AFS from dominant breaking waves on the sea drag, the impact being stronger the younger (and thus the steeper) are the seas. However, as found by Makin et al. (2004), the threshold approach is not universal, at least if the threshold value for the breaking wave steepness is assumed to be a universal constant.

In order to avoid an uncertainty with a choice of the threshold level, we shall define here $\Lambda(\mathbf{k})$ for the dominant waves in the manner similar to the equilibrium range. In stationary conditions, the energy balance equation for developing wind waves reads (e.g., Komen et al. 1994):

$$c_g \frac{\partial}{\partial x} E(\mathbf{k}) = N(\mathbf{k}) + I(\mathbf{k}) - D(\mathbf{k}), \tag{16}$$

where $E(\mathbf{k})$ is the wave energy spectral density, $N(\mathbf{k})$, $I(\mathbf{k})$, $D(\mathbf{k})$ are the energy sinks describing the non-linear four-wave interactions, wind energy input and dissipation due to wave breaking. As a well established fact (Komen et al. 1994), we note that the non-linear wave interactions (term N on the right-hand-side of (16)) provides the development of wind seas, i.e. the shifting of the spectral peak towards the low frequency with the increasing fetch. Therefore, in the vicinity of the spectral peak the energy balance Eq. 16 could be approximately reduced to

$$c_g \frac{\partial}{\partial x} E(\mathbf{k}) \simeq N(\mathbf{k}). \tag{17}$$

Then, in the vicinity of the peak, the wind energy input and dissipation due to wave breaking should be also balanced, at least in the order of magnitude

$$I(\mathbf{k}) \simeq D(\mathbf{k}) \tag{18}$$

(see Komen et al. (1994), their Figure 3.9). Referring to (14) and (18), we may expect that the expression for $\Lambda(\mathbf{k})$ in the spectral peak domain should have the same form (15) as for the equilibrium range. Thus we suggest that the spectral density of wave breaking fronts is defined by (15) in the full spectral range. Note, that the length of breaking fronts plays a crucial role in the present study defining both the sheltered area (9) and the separation stress (3). The validity of the adopted parameterization is restricted most likely by moderate wind speeds (< 20 m s^{-1}), and is questionable for strong or hurricane wind speeds. According to (15), in the equilibrium range of the wave spectrum $\Lambda(\mathbf{k})$ is a growing function of the wind speed, which at very high wind speeds should inevitably be saturated. From dimensional reasoning the length of breaking fronts should be saturated at

$$\Lambda(\mathbf{k}) \sim k^{-1}. \tag{19}$$

On the other hand, at very strong wind speeds generated foam and spume droplets result in the fact that the near surface layer becomes a two-phase "liquid", whose properties (e.g., density), differ significantly from the air. The interaction of this two-phase "liquid" with waves as well as the formation of the wave-induced and separation stress are not investigated so far. We leave these problems beyond the scope of the present study, relying on that extrapolation of (15) to high wind speeds will give the right trend in model results.

With the use of (15) Eq. 3 can be rewritten as

$$d\tau_s^0(\mathbf{k}) = c_s b^{-1} u_*^2 \cos^3 \theta k^{-2} \beta(\mathbf{k}) B(\mathbf{k}) d\mathbf{k}. \tag{20}$$

Thus, the equation for the sea surface drag (12) is the governing equation of the model, where the spectral density of the wave-induced $d\tau_w^0(\mathbf{k})$ and separation $d\tau_w^0(\mathbf{k})$ stress is defined by (2) and (20) correspondingly. The effect of the surface sheltering on the wave-induced and separation stress is taken into account through the cumulative sheltered area $q(k)$ defined by (9) and the Heaviside function $h(k_o - k)$ centered around the wavenumber k_o and determined as a solution of the equation $q(k_0) = 1$.

In this paper, as well as in KM01 and MK02, the saturation spectrum is defined as a sum $B(\mathbf{k}) = B_p(\mathbf{k}) + B_{eq}(\mathbf{k})$ of the dominant wave spectrum $B_p(\mathbf{k})$ with the shape proposed by Donelan et al. (1985), and the equilibrium spectrum $B_{eq}(\mathbf{k})$ with the shape proposed by Kudryavtsev et al. (1999)

$$B_{eq}(\mathbf{k}) = \alpha \left[\frac{\beta_\nu(\mathbf{k}) + (\beta_\nu^2(\mathbf{k}) + 4I_{pc}/\alpha)^{1/2}}{2} \right]^{1/n}, \tag{21}$$

where I_{pc} is the rate of the parasitic capillaries generation (which is vanished at $k < 2(g/T)^{1/2}$; T is the surface tension), $\beta_\nu = \beta - 4\nu k^2/\omega$ is the effective wave growth rate, which is the difference between the wind wave growth rate and the rate of viscous dissipation, α and n are the spectral parameters defined here as reported in Kudryavtsev et al. (2003) after the wave spectrum validation against the radar data. Similar to the wave-induced momentum flux we suggest that there is no wind energy input to short waves inside the sheltered area, i.e. the wind wave growth rate defining the shape of the spectrum (21) is

$$\beta(\mathbf{k}) = c_\beta [1 - q(k)](u_*/c)^2 \exp(-\varphi^2). \tag{22}$$

If for some scale of short waves $q(k) = 1$, i.e. they are totally covered by separation bubbles induced by longer waves, the wind energy flux to these waves vanishes, and thus their energy also vanishes. This corresponds to the suggestion by Donelan et al. (2004) that at high wind speeds the outer flow separating from continually breaking waves does not "see" the troughs of the long waves and is unable to generate small-scale roughness there.

4 Model results

4.1 Comparison with the laboratory experiment

Donelan et al. (2004) investigated in laboratory conditions the sea-surface drag at very high wind speeds. They found that the drag coefficient at wind speeds exceeding 30 m s^{-1} reaches saturation. The separation of the air flow from continually breaking dominant waves was suggested as the most plausible mechanism explaining this effect. The Donelan et al. (2004) experiment is simulated here by using the model described above.

The model wind speed dependence of the drag coefficient $C_{d10} = u_*^2/u_{10}^2$ is shown in Fig. 1a. The calculation of C_{d10} for infinite fetch is also shown. The wind speed dependence of C_{d10} below and above 20 m s^{-1} is quite different for limited and infinite fetch. For limited fetch the drag coefficient has a tendency for saturation, while for infinite fetch it continues to increase linearly. The model calculation of C_{d10} for limited fetch without accounting for the effect of sheltering is given in Fig. 1a by the dashed line. As expected the exclusion of this effect results in the overestimation of C_{d10}. Sheltering leads to the suppression of the surface drag. Model calculations are close to laboratory measurements by Donelan et al. (2004), their Fig. 2, that are shown in Fig. 1a by open circles (momentum budget method) and diamonds (Reynolds stress method). Though a systematic shift between the measurements
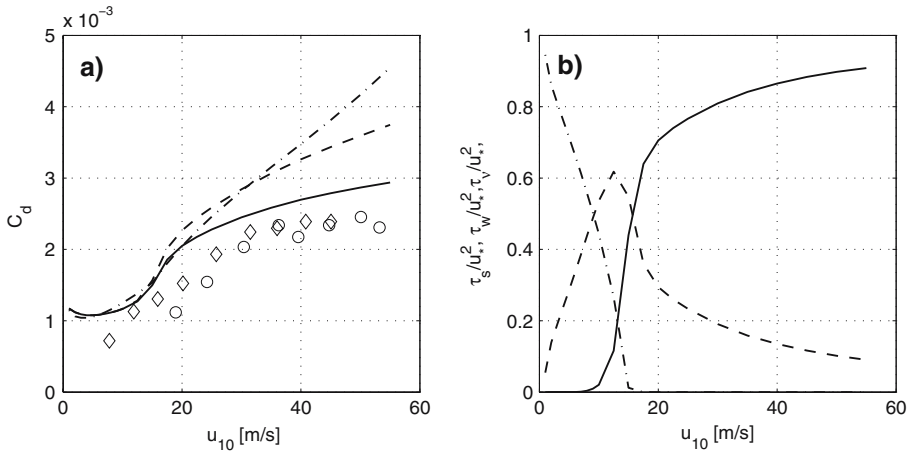
Fig. 1 (**a**) Drag coefficient C_{d10} versus wind speed u_{10}. Solid line, full model, limited fetch 10 m; dashed line, limited fetch 10 m, sheltering is switched off; dashed-dotted line, full model, infinite fetch. Laboratory measurements by Donelan et al. (2004) compiled from their Fig. 2 are shown by open circles (momentum budget method) and diamonds (Reynolds stress method) (**b**) Stress partitioning versus wind speed u_{10}. Solid line, stress due to separation; dashed line, wave-induced stress; dashed-dotted, viscous stress

and the model results is clearly observed, on the whole the model reproduces correctly a saturation trend in the distribution of C_{d10} at high wind speeds. We may consider this model result as an analogue of the C_{d10} saturation at high wind speeds revealed by Donelan et al. (2004) and interpret it as a result of the air-flow separation from continually breaking waves. The contribution of different components of the surface stress (viscous, wave-induced, and AFS) to the total stress is shown in Fig. 1b. At low wind speed $u_{10} < 5\,\text{m s}^{-1}$ the viscous stress τ_v dominates the stress, while at moderate wind speed of $5 < u_{10} < 15\,\text{m s}^{-1}$ that is the wave-induced stress τ_w. At higher wind speeds the impact of the AFS strongly increases, and at $u_{10} > 25\,\text{m s}^{-1}$ separation plays the crucial role in supporting stress providing the major part of the total stress (stresses in Fig. 1b are normalized on u_*^2, so that the total stress equals 1). This model result once again supports the suggestion by Donelan et al. (2004) that the separation from breaking waves leads to the saturation of the drag coefficient.

The role of sheltering by the AFS is further explained by Fig. 2, which shows the wind speed dependence of the total sheltered area $q(k_b)$ and the cumulative sheltered area $q(k)$. The total sheltered area is strongly wind speed dependent. At $u_{10} > 30\,\text{m s}^{-1}$ the AFS from breaking waves of different scales covers more than 75% of the surface area. As follows from Fig. 2b the most part of the sheltered area is produced by the AFS from waves of the spectral peak (the wavenumber of the spectral peak k_p for the corresponding wind speed is shown by vertical dashed lines, the lowest wavenumber corresponds to the highest wind speed). At highest wind speed the AFS from the spectral peak quenches the form drag from shorter scales for both the wave-induced and the AFS component, and thus is responsible for the total surface stress.

Donelan et al. (2004) investigated also the C-band (5.3 GHz) radar scattering for HH and VV polarizations at high wind speeds. Their measurements for HH polarization are shown in Fig. 3a by open circles (the signal at VV polarization is very similar to HH and thus not shown here). Note that the measured values of the radar cross-section are multiplied by the factor 2.2×10^{-2} to fit the plot for the saturation spectrum. As it follows from this plot,
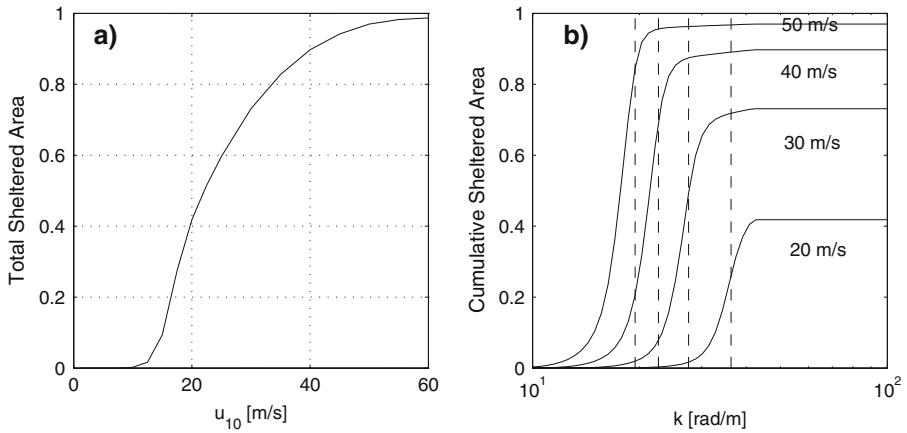
Fig. 2 Wind speed dependence of (**a**) the total sheltered area $q(k_b)$; and (**b**) the cumulative sheltered area $q(k)$. Dashed lines, the wavenumber of the spectral peak k_p for the corresponding wind speed, the lowest wavenumber corresponds to the highest wind speed
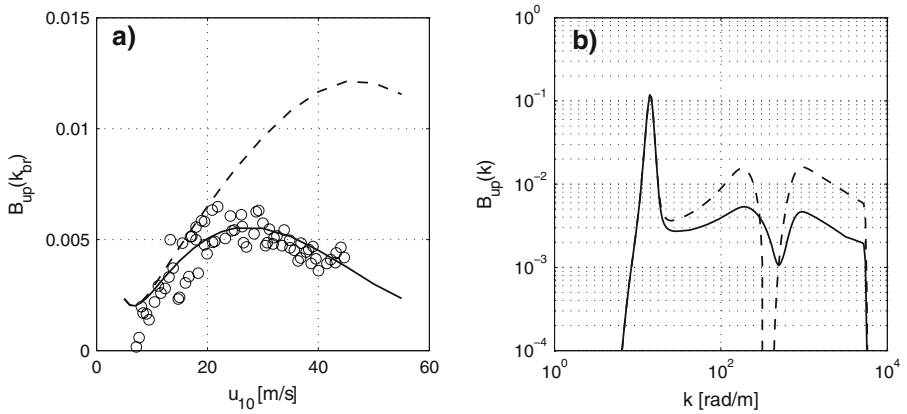

Fig. 3 (**a**) Wind speed dependence of the saturation spectrum in the wind direction at the C-band Bragg wavenumber. Solid line, full model; dashed line, sheltering is switched off. Open circles are measurements of the C-band radar cross section for HH polarization compiled from Donelan et al. (2004), their Fig. 5. Notice, that the measured values of the radar cross section are multiplied by factor 2.2×10^{-2}. (**b**) Spectral shape of the wave spectrum at $u_{10} = 30$ m s^{-1}. Solid line, full model; dashed line, sheltering is switched off

the radar signal associated with the geometric roughness of the centimetric waves reaches the maximum at the wind speed where the drag coefficient reaches the saturation level, and then decreases with the increase in the wind speed. As suggested, at very high wind speeds the air flow separating from continually breaking dominant wave crests no longer "sees" the troughs of these waves, and thus does not generate the small-scale roughness there, reducing the overall microwave reflectivity.

Qualitatively this mechanism is included in the wave spectrum model (21) through the reduction of the wind wave growth rate according to (22) due to sheltering by the AFS from dominant waves. Figure 3b illustrates the significance of the impact of the sheltering effect on the shape of the wave spectrum for laboratory conditions at $u_{10} = 30$ m s^{-1}. First, we note that the growth rate c_β depends on the aerodynamic roughness z_0 of the sea surface (see

notation for c_β in the text below Eq. 2). This is because the wind wave growth rate at the wavenumber k is proportional to the wind velocity squared at $z = \pi/k$ relative to the phase velocity. Therefore, the larger is z_0 the smaller is the growth rate. The dashed line in Fig. 3b shows the spectral shape when the effect of sheltering is not taken into account. The spectral gap in the vicinity of $k \sim (g/T)^{1/2}$ is caused by the weak wind energy input due to the high aerodynamic surface roughness (see Fig. 1a, dashed line). On the contrary, in the capillary range the spectral density does not vanish since these waves are parasitic capillaries, i.e. they are not dependent on the direct wind energy input to this spectral range. The solid line in Fig. 3b shows the spectral shape resulting from the full model. There is a dual effect of the AFS sheltering on the wave spectrum. On one hand it reduces the aerodynamic roughness (compare the solid and dashed lines in Fig. 1a) and thus the growth rate coefficient c_β is increased. As a result the spectral gap at $k \sim (g/T)^{1/2}$ is less pronounced. On the other hand sheltering of short waves by the AFS from breaking crests of longer waves decreases the effective growth rate that results in the reduction of the spectral level of short waves.

Figure 3a shows the wind speed dependence of the up-wind spectral level at the Bragg wavenumber (5.3 GHz) corresponding to the radar measurements by Donelan et al. (2004). Similar to observations, the spectrum of Bragg waves reaches maximum at 25 m s^{-1} and then decreases with increasing wind speed. This is because sheltering of the short Bragg wave by the AFS from breaking crests of longer waves decreases the effective growth rate of the Bragg wave and that results in the reduction of its spectral level. When sheltering is switched off the spectral level is considerably overestimated.

4.2 Aerodynamic and geometrical roughness at high winds

The experimental data and the model simulations indicate that the AFS from continually breaking dominant waves can be considered as a plausible mechanism explaining the saturation of the surface drag coefficient at high wind speeds. A question arises however as to how this mechanism works in real field conditions characterized by much longer fetches than in the laboratory? And can it explain a similar saturation and further reduction of the drag coefficient with increasing of the wind speed revealed by Powell et al. (2003) in tropical cyclones?

Figure 4 shows the model calculation of C_{d10} (in terms of the Charnock parameter $\alpha = z_0 g/u_*^2$) in a wide range of fetch from approximately 1m to 10^6 m and the wind speed from $10 \, \mathrm{m \, s^{-1}}$ to $50 \, \mathrm{m \, s^{-1}}$. In the range of fetch of practical interest ($X > 10^3$ m) and at the wind speed $u_{10} > 20 \, \mathrm{m \, s^{-1}}$ the model Charnock parameter appears to be almost independent of the fetch and the wind speed and approximately equal to $\alpha = 0.014$. At short fetches typical for the laboratory conditions α is considerably reduced. This regime of the air flow and the water surface interaction is described in the previous section.

Independence of α from the fetch and the wind speed in the range of long fetches is a surprising fact. To obtain a deeper insight, the contribution of different stress components to the total surface stress and the cumulative contribution of breaking wind waves to the sheltered area for various wind speeds at fetch 10^5 m are shown in Fig. 5. Unlike laboratory conditions, the separation stress τ_s and the wave-induced momentum flux τ_w contribute equally to the total stress at high wind speeds. Moreover, as follows from Fig. 5b, unlike very short fetches the dominant waves in this case do not contribute significantly to the sheltered area and to the AFS stress. At $X > 10^3$ m breaking of waves from the equilibrium range produces most of the AFS, and since they extract also most of the wave-induced momentum flux, we may conclude that the self-consistent interaction of the air flow with the equilibrium range of wind waves totally defines the form drag of the sea surface, in close relation to the Charnock prediction. No saturation or levelling off of C_{d10} (or suppression of the aerodynamic

Fig. 4 Charnock parameter $z_0 g/u_*^2$ versus fetch. Thin solid line, $u_{10} = 10$ m s^{-1}; dotted line, $u_{10} = 20$ m s^{-1}; dashed-dotted line, $u_{10} = 30$ m s^{-1}; dashed line, $u_{10} = 40$ m s^{-1}; solid line, $u_{10} = 50$ m s^{-1}
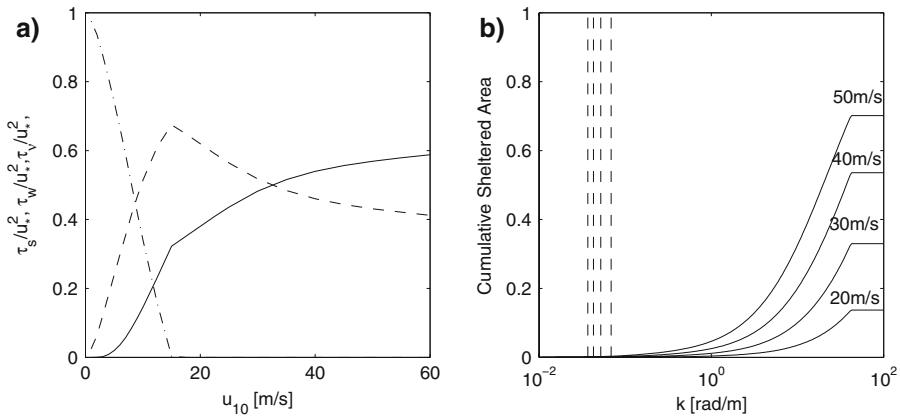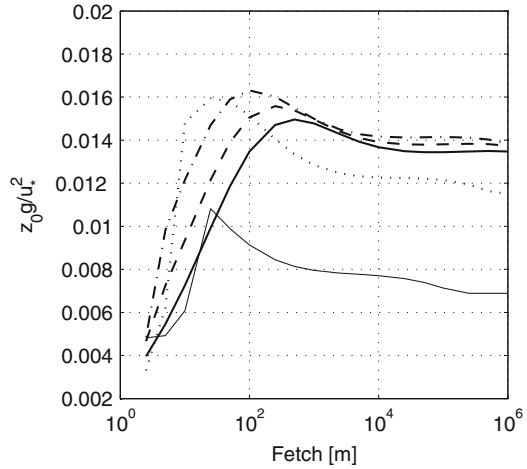
Fig. 5 (**a**) Stress partitioning versus wind speed. Solid line, stress due to separation; dashed line, wave-induced stress; dashed-dotted line, viscous stress. (**b**) Wind speed dependence of cumulative sheltered area $q(k)$. Dashed lines, the wavenumber of the spectral peak k_p for the corresponding wind speed, the lowest wavenumber corresponds to the highest wind speed. Fetch 10^5 m

roughness) is to be anticipated at high wind speeds if the wind fetch is long enough. Most probable that other mechanisms such as spray effects are responsible for the reduction of the drag coefficient in the field as observed by Powell et al. (2003) and showed by Makin (2005) and Kudryavtsev (2006).

Figure 6a shows a behaviour of the geometrical surface roughness, which is related to the saturation spectrum in the wind direction at the Bragg wavenumber in C- and L-band radar signals at high wind speeds. Unlike the aerodynamic roughness, the geometrical surface roughness demonstrates the apparent saturation around $u_{10} \simeq 30$ m s^{-1} with the following suppression (in C-band) at higher wind speeds. This behaviour is very similar to that revealed in laboratory conditions by Donelan et al. (2004) (compare with their Fig. 5). A physical mechanism leading to this behaviour is sheltering of short waves by the AFS from breaking longer waves. The sheltered area for C- and L-band roughness is shown in Fig. 6b. At highest wind speeds the sheltered area reaches 70% of the sea surface. According
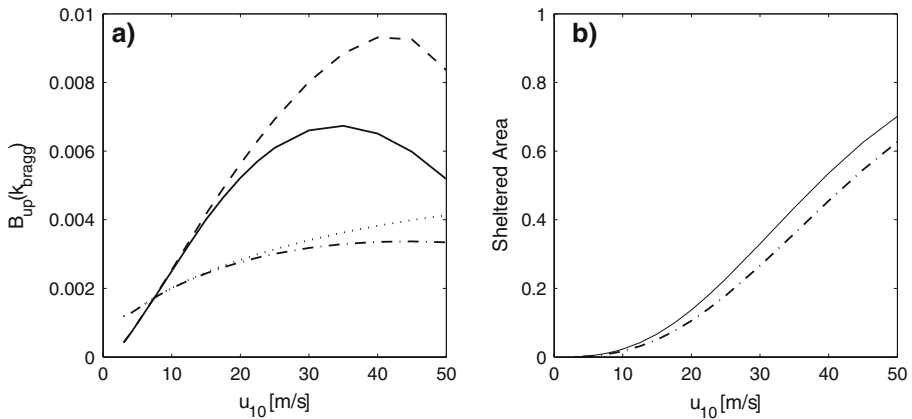
Fig. 6 (**a**) Wind speed dependence of the saturation spectrum in the wind direction at the Bragg wavenumber. Solid line, radar C-band (wavelength 0.06m), full model; dashed line, the same but sheltering is switched off; Dashed-dotted line, radar L-band (wavelength 0.20m); dotted line, the same but sheltering is switched off. (**b**) Wind speed dependence of the total sheltered area $q(k_b)$. Solid line, radar C-band; dashed-dotted line, L-band. Fetch 10^5 m

to the model, inside these areas the wind energy input to the short waves is suppressed, and thus their spectrum level is reduced. The model calculations of the wave spectral level without accounting for the sheltering effect are shown in Fig. 6a and demonstrate the significance of this mechanism.

Notice, that levelling off of the C-band radar signal at high wind speeds in the field conditions was revealed by Donnelly et al. (1999). This effect is included in the improved empirical ocean C-band backscatter model CMOD-5 (Hersbach 2003). Though the mechanism of radar scattering at high wind speeds is more complicated than the Bragg scattering model prediction (see, e.g., the discussion by Kudryavtsev et al. (2003) on the effect of wave breaking), our results clearly indicate that the effect of levelling off of the radar backscatter at high wind speeds results from the suppression of the geometrical surface roughness, and there is no need to invoke the suppression of the aerodynamic surface roughness to explain this phenomenon.

5 Conclusion

The current understanding of the physical processes at the sea surface at extreme wind conditions is based on few experiments performed in the field (Powell et al. 2003) and in the laboratory (Donelan et al. 2004). In both the saturation of the sea surface drag coefficient C_{d10} at very high wind speeds was revealed. One theoretical attempt to investigate this problem is based on the description of the sea droplets impact on the turbulent momentum flux and thus on the sea drag and was performed by Makin (2005), Bye and Jenkins (2006) and Kudryavtsev (2006). Though these studies showed strong potential ability of this mechanism in levelling off and further reduction of the drag coefficient at high wind speeds, the question remains what is the role of the surface roughness in the aerodynamic friction of the ocean surface at high wind speeds.

In this context, the laboratory study by Donelan et al. (2004) provides a good opportunity to answer this question. As concluded by Donelan et al. (2004) the saturation of the drag

coefficient in laboratory conditions could be explained by the saturation of the aerodynamic roughness due to the air flow separation from continually breaking waves. The role of water droplets in that study was not investigated (only the presence of droplets at highest winds was mentioned). However, one may anticipate that the impact of droplets on the air-flow dynamics at short fetches should be much weaker than in real field conditions, as (i) the range of breaking waves generating spume droplets is quite narrow (in laboratory conditions at highest wind speed the dominant wavelength was about 0.8 m) and thus the concentration of water droplets should be significantly lower that in field conditions, and (ii) generation of the vertical spread of the droplets and their possible influence on turbulence is confined to the internal boundary layer, which depth is about 3% of the fetch. So, the air flow with suspended droplets in laboratory conditions strongly differs from the air flow above ocean waves, where droplets can be transported by turbulence far away from the surface and thus strongly affecting the dynamics of the boundary layer.

In this paper based on the model developed by KM01 and MK02 we have investigated the effect of the surface roughness on the surface drag at high wind speeds. In the model, wind waves and the atmospheric boundary layer represent a coupled system. Waves provide the surface friction velocity through the form drag, while the energy input from the wind to waves depends on the friction velocity and the wind speed. Here, we extended the model to high wind speeds taking into account the effect of sheltering of short wind waves by the AFS from breaking crests of longer waves. It is suggested that the momentum and energy flux from the wind to short waves, which are trapped into the separation bubble of breaking longer waves, is locally vanished. On one hand, this leads to the reduction of the form drag due to the exclusion of contributions from these areas to the form drag supported by these short waves through the wave-induced momentum flux. On the other hand, in these sheltered areas the short waves do not receive energy from the wind and that reduces the wind wave growth rate, which defines the shape of the wave spectrum.

At short fetches, typical for laboratory conditions, and strong wind speeds steep dominant wind waves break very frequently and provide the major part of the total form drag through the AFS from breaking crests. At $u_{10} > 30$ m s^{-1} this contribution attains 90%, so that the effect of the short waves on the drag coefficient C_{d10} is considerably suppressed. This is a limiting regime when the aerodynamic roughness at short fetches is defined by the height of the dominant waves. In this case, the dependence of the drag coefficient on the wind speed is much weaker than would be anticipated from the standard parameterization of the roughness scale through the Charnock relation. This result is similar to the saturation of the drag coefficient at $u_{10} > 30$ m s^{-1} revealed experimentally by Donelan et al. (2004). According to the model, sheltering of the surface by the AFS from the dominant breaking waves prevents the energy flux to short waves, which in turn restrains their wind growth rate and leads to the reduction of the spectral level of the wave spectrum at the wind speed $u_{10} > 30$ m s^{-1}. This phenomenon was also found by Donelan et al. (2004) in the signature of radar measurements.

At long fetches representing the field conditions the spectral contribution of the wave components to the form drag is significantly changed as compared to the short fetches. Unlike the laboratory condition, waves of the spectral peak in the field are not so steep, thus they break rarely and their contribution to the AFS is weak. In this case, the surface form drag is determined predominantly by the AFS from breaking of the equilibrium range waves. Since the wave-induced momentum flux is supported to a large extent also by these waves, the aerodynamic roughness at high wind conditions becomes independent from the fetch and the wind speed. As shown, at high wind speeds up to 60 m s^{-1} the model aerodynamic roughness is consistent with the Charnock relation, i.e. no saturation of C_{d10} at high wind speeds can be explained by this mechanism if the fetch is long enough. Unlike the aerodynamic roughness,

the geometrical surface roughness (height of short wind waves) could be saturated or even suppressed when the wind speed exceeds $30 \, \mathrm{m \, s^{-1}}$. The effect is similar to that occurring at short fetches, and its origin is sheltering by the AFS from longer breaking waves that restraints the short wave growth rate. This mechanism can explain the effect of saturation of the C-band radar backscatter at high wind speeds found by Donnelly et al. (1999) in the field, which is adopted in the empirical geophysical backscatter model CMOD-5 (Hersbach 2003).

References

Babanin AV, Young IR (2005) Two-phase behaviour of the spectral dissipation of wind waves. In: Proceedings ocean waves measurement and analysis, fifth int sym WAVES 2005, 3–7 July, 2005, Madrid, Spain, Edge B, Santas JC, (eds) paper no. 51, 11

Banner ML (1990) The influence of wave breaking on the surface pressure distribution in wind wave interaction. J Fluid Mech 211:463–495

Banner ML, Melville WK (1976) On the separation of air flow above water waves. J Fluid Mech 77:825–842

Bye JAT, Jenkins AD (2006) Drag coefficient reduction at very high wind speeds. J Geophys Res 111, C033024, doi:10.1029/2005JC003114

Donelan MA, Hamilton J, Hui WH (1985) Directional spectra of wind generated waves. Phil Trans R Soc Lond, Ser A 315:509–562

Donelan MA, Haus BK, Reul N, Plant WJ, Stiassnie M, Graber HC, Brown OB, Saltzman ES (2004) On the limiting aerodynamic roughness of the ocean in very strong winds. Geophys Res Lett 31, L18306, doi:10.1029/2004GL019460

Donnelly WJ, Carswell JR, McIntosh RE, Chang PS, Wilkerson J, Marks F, Black PG (1999) Revised ocean backscatter models at C and Ku band under high-wind conditions. J Geophys Res 104:11485–11497

Emanuel KA (1995) Sensitivity of tropical cyclones to surface exchange coefficients and a revised steady-state model incorporating eye dynamics. J Atmos Sci 52:3969–3976

Giovanangeli JP, Reul N, Garat MH, Branger H (1999) Some aspects of wind-wave coupling at high winds:an experimental study. In: Wind-over-wave couplings. pp 81–90, Clarendon Press, Oxford 356 pp

Hersbach H (2003) CMOD5 an improved geophysical model function for ERS C-band scatterometry,/ Techn. Mem./, ECMWF, Reading, UK

Kawamura H, Toba Y (1988) Ordered motions in the turbulent boundary layer over wind waves. J Fluid Mech 197:105–138

Komen GJ, Cavalery L, Donelan M, Hasselmann K, Hasselmann S, Janssen PAEM (1994) Dynamics and modelling of ocean waves. Cambridge University Press, 540 pp

Kudryavtsev VN (2006) On effect of sea drops on atmospheric boundary layer. J Geophys Res 111: C07020, doi:10.1029/2005JC002970

Kudryavtsev VN, Makin VK (2001) The impact of air-flow separation on the drag of the sea surface. Boundary-Layer Meteorol 98:155–171

Kudryavtsev VN, Makin VK, Chapron B (1999) Coupled sea surface-atmosphere model 2. Spectrum of short wind waves. J Geophys Res 104:7625–7639

Kudryavtsev V, Hauser D, Caudal G, Chapron B (2003) A semi-empirical model of the normalized radar cross-section of the sea surface. Part 1: The background model. J Geophys Res 108(C3):8054, doi:10.1029/2001JC001003

Lonquet-Higgins MS (1957) The statistical analysis of a random moving surface. Phil Trans R Soc Lond, Ser A 249:321–387

Makin VK (2005) A note on drag of the sea surface at hurricane winds. Boundary-Layer Meteorol 115:169–176

Makin VK, Kudryavtsev VN (1999) Coupled sea surface- atmosphere model 1. Wind over waves coupling. J Geophys Res 104:7613–7623

Makin VK, Kudryavtsev VN (2002) Impact of dominant waves on sea drag. Boundary-Layer Meteorol 103:83–99

Makin VK, Caulliez G, Kudryavtsev VN (2004) Drag of the water surface at limited fetch: laboratory measurements and modelling. In: Geophysical research abstracts 1016, EGU04-A-00113, EGU General Assembly, April 25–31, 2004, Nice, France

Melville WK (1996) The role of surface-wave breaking in air-sea interaction. Ann Rev Fluid Mech 28:279–321

Monin AS, Yaglom AM (1971) Statistical fluid mechanics, vol 1. Cambridge: MIT Press 769 pp

Reul N, Branger H, Giovanangeli JP (1999) Air flow separation over unsteady breaking waves. Physics of Fluids 11:1959–1961

Phillips OM (1985) Spectral and statistical properties of the equilibrium range in wind generated gravity waves. J Fluid Mech 156:505–531

Powell MD, Vickery PJ, Reinhold TA (2003) Reduced drag coefficient for high wind speeds in tropical cyclones. Nature 422:279–283